An Improved [211]At-Labeled Agent for PSMA-Targeted α-Therapy

Ronnie C. Mease[1], Choong Mo Kang[2], Vivek Kumar[1], Sangeeta Ray Banerjee[1], Il Minn[1], Mary Brummet[1], Kathleen L. Gabrielson[3], Yutian Feng[2], Andrew Park[1], Ana P. Kiess[4], George Sgouros[1,4], Ganesan Vaidyanathan[2], Michael R. Zalutsky[2], and Martin G. Pomper[1,4]

[1]Russell H. Morgan Department of Radiology and Radiological Science, Johns Hopkins University School of Medicine, Baltimore, Maryland; [2]Department of Radiology, Duke University Medical Center, Durham, North Carolina; [3]Department of Molecular and Comparative Pathobiology, Johns Hopkins University School of Medicine, Baltimore, Maryland; and [4]Department of Radiation Oncology and Molecular Radiation Sciences, Johns Hopkins University School of Medicine, Baltimore, Maryland

α-Particle emitters targeting the prostate-specific membrane antigen (PSMA) proved effective in treating patients with prostate cancer who were unresponsive to the corresponding β-particle therapy. [211]At is an α-emitter that may engender less toxicity than other α-emitting agents. We synthesized a new [211]At-labeled radiotracer targeting PSMA that resulted from the search for a pharmacokinetically optimized agent. **Methods:** A small series of ^{125}I-labeled compounds was synthesized from tin precursors to evaluate the effect of the location of the radiohalogen within the molecule and the presence of lutetium in the chelate on biodistribution. On that basis, [211]At-**3**-Lu was selected and evaluated in cell uptake and internalization studies, and biodistribution and PSMA-expressing (PSMA+) PC3 PIP tumor growth control were evaluated in experimental flank and metastatic (PC3-ML-Luc) models. A long-term (13-mo) toxicity study was performed for [211]At-**3**-Lu, including tissue chemistries and histopathology. **Results:** The radiochemical yield of [211]At-**3**-Lu was 17.8% ± 8.2%. Lead compound [211]At-**3**-Lu demonstrated total uptake within PSMA+ PC3 PIP cells of 13.4 ± 0.5% of the input dose after 4 h of incubation, with little uptake in control cells. In SCID mice, [211]At-**3**-Lu provided uptake that was 30.6 ± 4.8 percentage injected dose per gram (%ID/g) in PSMA+ PC3 PIP tumor at 1 h after injection, and this uptake decreased to 9.46 ± 0.96 %ID/g by 24 h. Tumor–to–salivary gland and tumor-to-kidney ratios were 129 ± 99 at 4 h and 130 ± 113 at 24 h, respectively. Deastatination was not significant (stomach, 0.34 ± 0.20 %ID/g at 4 h). Dose-dependent survival was demonstrated at higher doses (>1.48 MBq) in both flank and metastatic models. There was little off-target toxicity, as demonstrated by hematopoietic stability, unchanged tissue chemistries, weight gain rather than loss throughout treatment, and favorable histopathologic findings. **Conclusion:** Compound [211]At-**3**-Lu or close analogs may provide limited and acceptable toxicity while retaining efficacy in management of prostate cancer.

Key Words: prostate cancer; α-emitter; radiopharmaceutical therapy; [211]At; PSMA; murine models

Radiopharmaceutical therapy targeting prostate-specific membrane antigen (PSMA) using low-molecular-weight agents is becoming viable for metastatic prostate cancer (*1–3*). Such treatments have used β-particle emitters, including ^{131}I and ^{177}Lu, or α-particle emitters such as [213]Bi, [212]Pb, [227]Th, and [225]Ac (*4–10*). To date, most clinical trials have used [177]Lu. In one such trial, PSA levels decreased by over 50% in 57% of patients (*11*). PSMA-targeted α-particle emitters may be even more promising, as evidenced by treatment with an [225]Ac-labeled agent producing a significant tumor response in patients who were unresponsive to prior β-emitter therapy (*12,13*). However, the side effect of xerostomia from uptake of the agents in the salivary glands, and the potential of long-term renal toxicity, remain possible limitations.

A possible issue with α-emitters such as [225]Ac is that multiple α-emitting daughters are generated from α-emitting parents, and in each case the energy imparted by the nuclear recoil effect is orders of magnitude greater than chemical bonds. That energy makes the release of the radioactive daughters from the targeting vector extremely likely, which can then lead to unintended irradiation of nontarget tissues (*14,15*). Our approach has been to use the radiohalogen [211]At, which emits a single α-particle per decay. That strategy may permit greater control on the targeting of the therapeutic radiation, thereby reducing the chance of off-target effects. It should be noted that 58% of the α-particles emitted during [211]At decay do involve a chemical transformation of astatine to polonium before α-emission. In that case, the parent decays by electron capture, not α-emission; the α-emitting 0.52-s half-life [211]Po daughter is therefore not nuclear-recoil–afflicted. Even with worst-possible-case assumptions—that [211]Po escapes immediately from the cell surface and can freely diffuse—nearly 100% of [211]Po atoms should decay within 2 cell diameters from the original cell surface (*16*). The second [211]At decay branch (42%) is by direct α-particle emission to [207]Bi, which has a 32.9-y half-life. That long-lived radioactive daughter is not of concern because about 100,000 decays of [211]At are needed to produce a single decay of [207]Bi. Accordingly, a 370-MBq (10 mCi) hypothetical patient dose of an [211]At-labeled PSMA agent would yield approximately 3.7 kBq (~0.1 μCi) of [207]Bi, a level that is only 0.1% of the annual limit of intake recommended for [207]Bi by the Nuclear Regulatory Commission (3.7 MBq [100 μCi]) (*17*). Despite these issues, we believe [211]At remains the best option for α-therapy.

Our previous studies used the following compounds, shown in Figure 1: DCABzL, HS-549, GV-620, GV-904, and YC-550. The initial compound studied, [211]At-DCABzL, showed high and prolonged uptake in PSMA-expressing (PSMA+) tumor xenografts and renal cortex, with moderate uptake in thyroid and stomach, likely from dehalogenation (18). Despite that suboptimal biodistribution, we were able to demonstrate a treatment-related increase in survival in both flank tumor xenograft and micrometastatic models with a single dose of 0.74 MBq (20 μCi) and 0.11–0.37 MBq (3–10 μCi), respectively (18). From long-term toxicity studies, we determined that the dose-limiting toxicity was late radiation nephropathy (18). Using the [211]At-labeled analogs YC-550, HS-549, GV-904, and GV-620 (Fig. 1), we observed faster renal clearance in mice than was seen with [211]At-DCABzL. However, in vivo dehalogenation or off-target organ uptake remained an issue (19).

Here, we describe a new [211]At-labeled PSMA-targeted compound with high stability in vivo and rapid clearance from off-target tissues (including kidneys, salivary and lacrimal glands) in mice. We also demonstrate a dose-dependent therapeutic effect in flank xenograft and metastatic tumor models of prostate cancer.

MATERIALS AND METHODS

Reagents, Cell Lines, and Animal Models

Chemistry. The syntheses of compounds 4 (Fig. 1) and its tin precursor, 15, as well as of unlabeled compounds 3, 3-Lu, and their tin precursor, 9, are outlined in Figures 2 and 3 and are described in detail in the supplemental materials (available at http://jnm.snmjournals.org [20–22]). The PSMA-binding affinity of compounds 3 and 4 was determined using a fluorescence-based assay we have previously reported (18).

Radiochemistry. Sodium ^{125}I-iodide in 10 μM NaOH (pH 8–11) was purchased from Perkin Elmer. [211]At was produced on the Duke University CS-30 cyclotron via the [209]Bi(α,2n)[211]At reaction on natural bismuth targets (23,24).

We investigated 2 methods (A and B) for the preparation of ^{125}I-3-Lu and [211]At-3-Lu (Fig. 2). Method A included purification of ^{125}I/[211]At-3 before complexation with [175]Lu(III), whereas in method B lutetium complexation was performed in situ without purification of the intermediate. In both methods, the final compound was purified by high-performance liquid chromatography. Radiosynthesis of [211]At-3-Lu by method B began with a solution of [211]At in 0.02% N-chlorosuccinimide in methanol (600 μL; 638 MBq [17.3 mCi]) that was added to 310 μg (204 nmol) of compound 9 in a borosilicate screw cap vial followed by 12 μL of glacial acetic acid. The vial was capped, shaken, and allowed to stand at room temperature for 10 min. The reaction mixture was concentrated to dryness using a stream of nitrogen at 60°C. A 95:5 mixture of trifluoroacetic acid:water (200 μL) was added, and the vial was heated at 60°C for 30 min. Volatiles were evaporated using a stream of nitrogen at 60°C. Sodium acetate buffer (0.1 M), pH 4.5 (500 μL), and a solution of $Lu(NO_3)_3$ in 0.1 M HCl (65 μL; 325 nmol) were added to the residue, and the solution was mixed with a micropipette. That solution was heated at 60°C for 20 min, 100 μL of 5 mM ethylenediaminetetraacetic acid was added, and the reaction mixture was diluted with 600 μL of water. The final product was purified by high-performance liquid chromatography. For this, a Phenomenex Luna C18 column (250 × 4.6 mm, 10 μm) was eluted at a flow rate of 1 mL/min with a gradient consisting of 0.1% trifluoroacetic acid in both water (solvent A) and acetonitrile (solvent B). The proportion of B was linearly increased from 15% to 40% over 30 min. Under those conditions, [211]At-3-Lu [54 MBq (1.47 mCi)] eluted at 22.5 min. Pooled high-performance liquid chromatography fractions containing [211]At-3-Lu were diluted to 20 mL with water and were loaded onto a Waters Oasis HLB Light Sep-Pak. The cartridge was washed with 5 mL of water and dried under a stream of nitrogen, and the product was eluted with 0.5 mL of ethanol. The eluate was concentrated using a stream of nitrogen, and the activity was reconstituted in saline. Detailed radiosyntheses of [211]At-3-Lu by method A, and syntheses of ^{125}I-3, ^{125}I-3-Lu, ^{125}I-4, and ^{125}I-4-Lu, are presented in the supplemental materials. Radiolabeling yields for ^{125}I/[211]At-3 and ^{125}I/[211]At-3-Lu are summarized in Tables 1 and 2.

Cell Lines and Culture Conditions. PSMA+ PC3 PIP and PSMA-negative (PSMA−) PC3 flu cells were maintained as previously described (25–27). For the experimental metastatic model, parental PC3-ML-Luc cells were obtained from Dr. Mauricio Reginato (Drexel University). Those cells are characterized in Supplemental Figure 1. Cell lines were maintained *Mycoplasma*-free through biweekly testing with the MycoAlert *Mycoplasma* detection kit (Lonza).

Animals. Animal studies conformed to protocols approved by the Johns Hopkins Animal Care and Use Committee. Johns Hopkins University has an approved Public Health Service Policy, and the approved protocols follow this and Animal Welfare Act regulations. NSG (NOD/SCID/IL2Rγnull) mice were obtained from the Animal Resources Core of the Johns Hopkins Sydney Kimmel Comprehensive Cancer Center.

In Vitro Studies

PSMA+ PC3 PIP cells were plated at 5×10^5 cells per well and incubated overnight. Cells were then incubated with [211]At-3 in medium (~3.7 kBq/100 μL) at 37°C for 0.5, 1.0, 2.0, and 4.0 h. Cell culture supernatant was removed, and the cells were processed as before (18). Cell-associated radioactivity was calculated as percentage of input dose. The
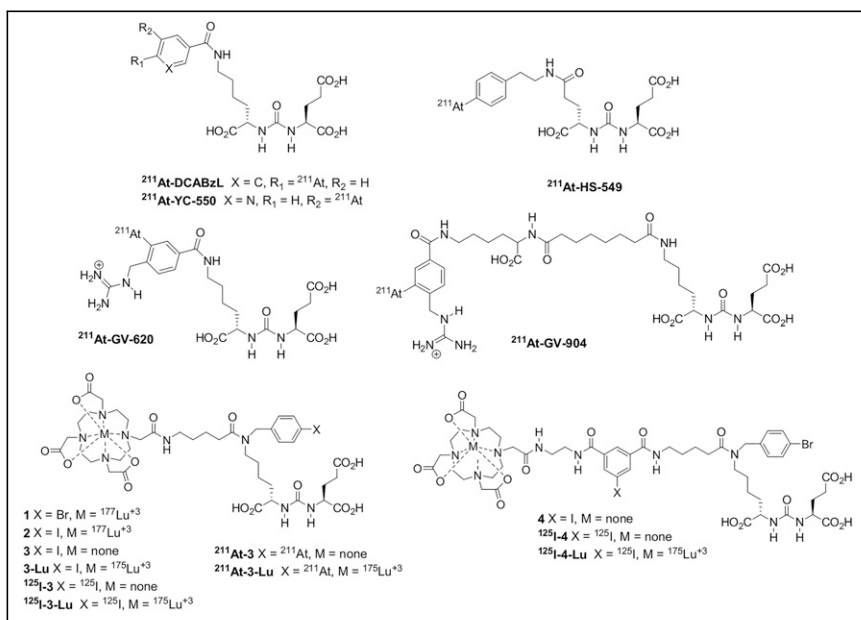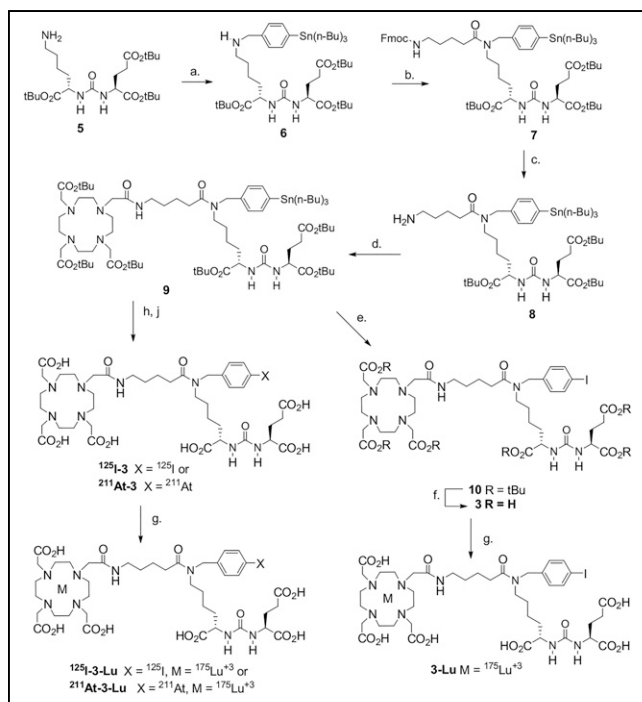

FIGURE 1. PSMA-targeted agents.

FIGURE 2. Synthesis of compound 3, 3-Lu, radiolabeling of precursor 9, ^{125}I-3, ^{125}I-3-Lu, and ^{211}At-3-Lu. Reagents and conditions: 4-(tributyl-stannyl)benzaldehyde, methanol, sodium cyanoborohydride (a); 5-(Fmo-c-amino)valeric acid, O-(N-succinimidyl)-N,N,N',N'-tetramethyluronium tetrafluoroborate, N,N-diisopropylethylamine, dimethylformamide (b); 20% piperidine in dimethylformamide (c); DOTA-N-hydroxysuccinimide tri-tert-butylester, N,N-diisopropylethylamine, dimethylsulfoxide (d); I$_2$, CH$_2$Cl$_2$ (e); 1/1 trifluoroacetic acid/CH$_2$Cl$_2$ (f); 0.2 M NH$_4$OAc, dimethyl-sulfoxide, 5 mM ^{175}Lu(NO$_3$)$_3$·H$_2$O in 0.1N HCl, 70°C, 20 min (g, step i), ethylenediaminetetraacetic acid (g, step ii); Na^{125}I or ^{211}At, methanol, gla-cial acetic acid, room temperature, 20 min (h); and trifluoroacetic acid, 60–70°C, 30–45 min (j).

internalized fraction of radioactivity was determined by solubilizing cells with 1% SDS cell lysis buffer after removing the unbound fractions and cell surface–bound fractions (by washing with glycine-HCl buffer). To determine binding specificity, PSMA+ PC3 PIP cells were coincubated with ^{211}At-3 and the known PSMA inhibitor (R, S)-2-(phosphonomethyl)pentanedioic acid (100 μM) (28).

In Vivo Studies

Biodistribution. Six- to 8-wk-old male NSG mice were implanted subcutaneously with PSMA+ PC3 PIP (1.5×10^6) and PSMA− PC3 flu cells (1×10^6) in 100 μL of Hanks balanced salt solution (Cellgro; Corning) at the forward right and left flanks, respectively. Mice were used in ex vivo biodistribution assays when the xenografts reached 5–7 mm in diameter. Biodistribution experiments were performed in the above mice bearing both PSMA+ PC3 PIP and PSMA− PC3 flu flank xenografts after an intravenous bolus of 37 kBq (1 μCi) of ^{125}I-4, ^{125}I-4-Lu, ^{125}I-3, ^{125}I-3-Lu, or ^{211}At-3-Lu. Tissues harvested at 1, 4, and 24 h after injection ($n = 5$ per time point) included blood, heart, lung, liver, spleen, pancreas, stomach, small intestine, large intestine, fat, muscle, salivary gland, lacrimal gland, kidney, bladder, PSMA+ PC3 PIP tumor, and PSMA− PC3 flu tumor. Each tissue was weighed, and the associated radioactivity was measured with an automated γ-counter (2480 Wizard; Perkin Elmer). The percentage injected dose (%ID) was calculated using a known dilution of %ID. All measurements were corrected for decay. Data are expressed as %ID/g of tissue or per organ (%ID) for organs that were too small for accurate dissection. All data are expressed as mean ± SD.

Antitumor Efficacy in Subcutaneous Xenograft Model. PSMA+ PC3 PIP and PSMA− PC3 flu cells were implanted subcutaneously in male NSG mice as described above. When tumor diameter reached 5–7 mm, a single intravenous injection was performed with saline or with 0.24 MBq (6.6 μCi), 0.74 MBq (20 μCi), 1.48 MBq (40 μCi), or 3.7 MBq (100 μCi) of ^{211}At-3-Lu ($n = 5$ per group). Tumor progression was monitored by measuring subcutaneous tumor volume [(width$^2 \times$ length)/2 mm^3] using a caliper. A tumor volume increase of more than 4-fold was scored as death of the animal, at which point it was euthanized.

Antitumor Efficacy in Metastatic Model. Four- to 6-wk-old NSG mice were injected intravenously with 1×10^6 PC3-ML-Luc cells suspended in 200 μL of Hanks balanced salt solution to form micrometastatic deposits. One week after injection of cells, the mice were injected intravenously with 0 MBq (0 μCi; saline), 0.185 MBq (5 μCi), 0.37 MBq (10 μCi), 0.74 MBq (20 μCi), 1.48 MBq (40 μCi), or 3.7 MBq (100 μCi) of ^{211}At-3-Lu ($n = 5$ per group). Metastatic tumor progression was monitored by in vivo bioluminescence imaging and survival of injected animals. Weekly bioluminescence imaging was performed using the IVIS Spectrum in vivo imager (Perkin-Elmer). Mice were sacrificed and scored as death if they lost more than 20% of body weight or had signs of discomfort, such as hunched posture, anorexia, or dehydration. For both animal models, the probability of survival was characterized by Kaplan–Meier curves using Prism software (GraphPad Software).

Long-Term Toxicity. Healthy 11-wk-old male CD1 mice (Charles River) weighing 35–40 g received intravenous injections of 0 MBq (0 μCi; saline), 0.24 MBq (6.6 μCi), 0.74 MBq (20 μCi), or 1.48 MBq (40 μCi) of ^{211}At-3-Lu ($n = 5$ per group). Mice were monitored for 13 mo with a health inspection daily and a weight measurement twice per week. Monthly urinalysis was performed for specific gravity and urine protein content using Chemstrip test strips (Roche Diagnostics). After 13 mo, the mice were euthanized in a CO$_2$ chamber, and blood, kidney, salivary glands, and lacrimal glands were collected. Complete blood counts, including white blood cells, red blood cells, hemoglobin, hematocrit, mean corpuscular volume, mean corpuscular hemoglobin, mean corpuscular hemoglobin concentration, and platelets, were measured using the scil Vet ABC hematology analyzer (scil Animal Care Co.). Blood chemistry testing for blood urea nitrogen, glucose, alkaline phosphatase, total protein, alanine aminotransferase, and creatinine was performed using a Spotchem EZ chemistry analyzer (Arkray USA). Histopathologic evaluation was performed by a certified veterinary pathologist for kidneys, salivary glands, and lacrimal glands with hematoxylin and eosin–stained slides of each tissue.

Statistics

Survival analyses for the metastatic and subcutaneous models were performed using Prism software (version 9; GraphPad Software). P values were calculated by the log-rank (Mantel–Cox) test and were considered significant if less than 0.05.

RESULTS

Chemistry

Because of the promising results obtained with ^{177}Lu-1 and ^{177}Lu-2, our strategy was to replace the nonradioactive bromine or iodine atom with ^{125}I and evaluate their biodistribution in tumor-bearing animals with or without chelated nonradioactive lutetium (^{125}I-3 and ^{125}I-3-Lu [inhibition constant, 0.09–34 nM (29)]; Fig. 2). For comparison, we also synthesized and evaluated ^{125}I-4 and ^{125}I-4-Lu (Fig. 3), where the radioiodine was
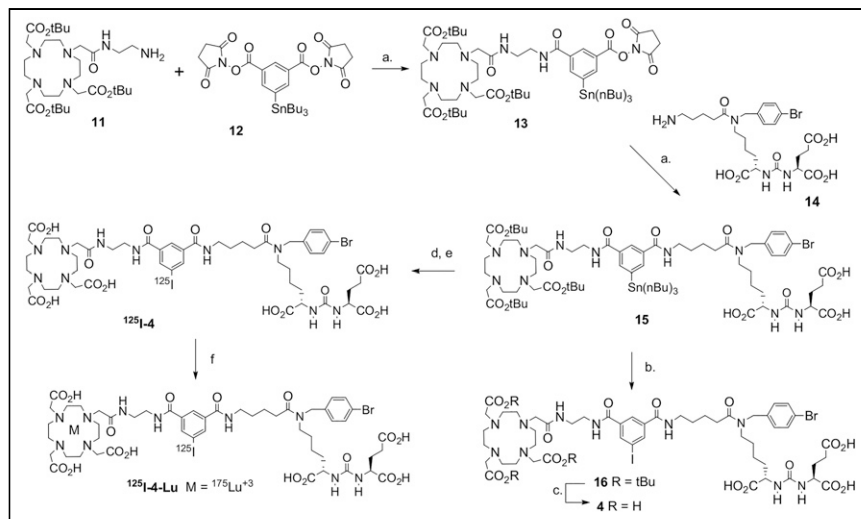
FIGURE 3. Synthesis of radiolabeling precursor 15, 4, ^{125}I-4, and ^{125}I-4-Lu. Reagents and conditions: triethylamine, dimethylsulfoxide, room temperature, 2 h (a); I$_2$, CH$_2$Cl$_2$, room temperature, 2 h (b); 1/1 trifluoroacetic acid/CH$_2$Cl$_2$, room temperature, 2 h (c); Na^{125}I, N-chlorosuccinimide, glacial acetic acid, methanol, room temperature, 20 min (d); concentrated formic acid, 60°C, 1 h (e); 0.1 M sodium acetate, pH 4.5, 5 mM ^{175}Lu(NO$_3$)$_3$ in 0.1 M HCl, 60°C, 20 min (f, step i); and 5 mM ethylenediaminetetraacetic acid (f, step ii).

incorporated into the linking group, and each contained a 4-bromobenzyl moiety as in compound 1. The ^{211}At-labeled analog of the most promising iodinated compound was synthesized and evaluated. The binding affinity of unlabeled compounds 3 and 4 was as follows: half-maximal inhibitory concentration, 1.51 nM (95% CI, 0.62–3.64 nM); inhibition constant, 0.30 nM (95% CI,

0.13–0.73 nM), and half-maximal inhibitory concentration, 7.82 nM (95% CI, 6.16–9.94 nM); inhibition constant, 0.30 nM (95% CI, 1.23–1.99 nM), respectively.

Radiochemistry

Syntheses of ^{125}I-4 and ^{125}I-4-Lu were each performed once. The yield of ^{125}I-4 from ^{125}I-iodide was 14%, and that for the conversion of ^{125}I-4 to ^{125}I-4-Lu was 82%. Radiolabeling conditions and yields for ^{125}I/^{211}At-3 and ^{125}I/^{211}At-3-Lu are given in Tables 1 and 2, respectively. In general, fresh batches of ^{211}At provided higher overall yields of either compound. Purification of the nonmetallated intermediate (^{125}I/^{211}At-3) did not enhance yield and actually provided lower overall yields of the final product (^{125}I/^{211}At-3-Lu).

Cell Uptake and Internalization

In vitro studies of ^{211}At-3-Lu demonstrated total uptake within PSMA+ PC3 PIP cells of 13.4% ± 0.5% of the input dose after 4 h of incubation and an increasing internalized fraction over time, namely, 15.8% ± 0.7%, 19.0% ± 0.7%, 24.5% ± 1.0%, and 27.7% ± 2.2% at 0.5, 1.0, 2.0, and 4.0 h, respectively. Coincubation with (R, S)-2-(phosphonomethyl)pentanedioic acid showed an average of 0.6% uptake at all time points, confirming PSMA-specific uptake (Supplemental Fig. 2) (18).

TABLE 1
Radiolabeling Yields for ^{125}I/^{211}At-3

Radionuclide	Starting radioactivity	Age of ^{211}At	n	% yield*
^{125}I	0.036–0.266 GBq (0.96–7.2 mCi)	Not applicable	3	56.1 ± 13.7
^{211}At	0.1628–0.3145 GBq (4.4–8.5 mC)i	Fresh	3	49.6 ± 6.8
^{211}At	0.444–0.6623 GBq (12.0–17.9 mCi)	≥9 h	2	20.8% ± 8.2%

*After preparative high-performance liquid chromatography purification.

TABLE 2
Radiolabeling Yields for ^{125}I/^{211}At-3-Lu

Radionuclide	Starting radioactivity	Age of ^{211}At	Method of preparation	n	% yield*
^{125}I	0.170–0.266 GBq (4.6–7.2 mCi)	Not applicable	A	2	46.5 ± 7.7
^{125}I	0.054–0.518 GBq (1.47–14 mCi)	Not applicable	B	4	62.8 ± 9.0
^{211}At	0.16–0.31 GBq (4.4–8.5 mCi)	Fresh	A	3	6.3 ± 1.8
^{211}At	0.126- 0.34 GBq (3.4–9.2 mCi)	Fresh	B	2	17.8 ± 8.2
^{211}At	0.44–0.66 GBq (12.0–17.0 mCi)	≥9 h	A	2	8.6 ± 3.6
^{211}At	0.115–0.877 GBq (3.1–23.7 mCi)	≥9 h	B	4	13.6 ± 8.4

*After preparative high-performance liquid chromatography purification.
A = separate preparative high-performance liquid chromatography purification of ^{125}I/^{211}At-3 and ^{125}I/^{211}At-3-Lu. B = preparative high-performance liquid chromatography purification of ^{125}I/^{211}At-3-Lu only.

Biodistribution

Detailed biodistribution data, represented as %ID/g for all radio-labeled compounds, are given in Supplemental Tables 1–6. There was little deastatination of ^{211}At-3-Lu in vivo as evidenced by low uptake of radioactivity in stomach (0.39 ± 0.12 %ID/g), salivary glands (0.47 ± 0.19 %ID/g), and spleen (2.51 ± 0.94 %ID/g) at 1 h after administration, which decreased further by 4 h for stomach and salivary glands (<0.05 %ID/g in spleen) (Supplemental Table 3). Uptake in PSMA+ PC3 PIP tumor and selected nontarget organs is shown in Figure 4. All compounds had high tumor uptake at 1 h (30–60 %ID/g). Although tumor activity remained at that high level out to 24 h for ^{125}I-4, ^{125}I-4-Lu, and ^{125}I-3, 50% and 67% of ^{125}I-3-Lu and ^{211}At-3-Lu activity, respectively, cleared from the tumor by 24 h. Importantly, ^{211}At-3-Lu was nearly undetectable in normal organs at 24 h. Renal uptake of ^{211}At-3-Lu at 1 h (89.5 ± 42.7 %ID/g) was 30%–50% lower than that seen for other compounds. By 4 h, renal activity levels for ^{125}I-3-Lu and ^{211}At-3-Lu decreased to 18.2 ± 3.9 and 2.1 ± 0.6 %ID/g, respectively, whereas activity in kidneys for the other compounds remained high (162–199 %ID/g). By 24 h, activity in kidneys from ^{125}I-3-Lu and ^{211}At-3-Lu decreased to 3.30 ± 1.15 %ID/g and 0.02 ± 0.20 %ID/g, respectively. On the other hand, renal activity was 141 ± 18, 50.4 ± 25.9, and 30.6 ± 14.0 %ID/g for ^{125}I-4, ^{125}I-4-Lu, and ^{125}I-3, respectively. Despite the lower %ID/g values of ^{211}At-3-Lu in tumor, its considerably faster renal clearance resulted in tumor-to-kidney ratios of 8 and 130 at 4 and 24 h, respectively (Fig. 5). Those values are roughly 5- and 16-fold higher than achieved with ^{125}I-3-Lu and 20- to 200-fold higher than achieved with the other compounds. The uptake in spleen at 1 h was much lower for ^{125}I-3-Lu and ^{211}At-3-Lu (7.41 ± 2.57 and 2.51 ± 0.94 %ID/g, respectively) than for the other compounds (40–70 %ID/g). Radioactivity from spleen cleared rapidly for all agents, resulting in tumor-to-spleen ratios at 4 h of 1.3, 4.4, 6.8, 43, and 97 for ^{125}I-4, ^{125}I-4-Lu, ^{125}I-3, ^{125}I-3-Lu, and ^{211}At-3-Lu, respectively. The uptake of ^{125}I-3-Lu and ^{211}At-3-Lu in salivary and lacrimal glands was lower than observed for any other compound at any time point, resulting in tumor–to–salivary gland ratios of 58 and 75 and tumor–to–lacrimal gland

ratios of 13 and 44 at 1 h after injection, respectively (Supplemental Tables 5 and 6, respectively). At 4 h, those values were 365 and 129 for salivary gland and 92 and 164 for lacrimal gland.

α-Therapy with ^{211}At-3-Lu

We first evaluated the efficacy of ^{211}At-3-Lu by scoring growth inhibition of subcutaneous xenograft tumors of both PSMA+ PC3 PIP and PSMA− PC3 flu cells implanted in the same animal. A single intravenous injection of 4 different doses (0 MBq [0 µCi; saline], 0.24 MBq [6.5 µCi], 0.74 MBq [20 µCi], 1.48 MBq [40 µCi], or 3.7 MBq [100 µCi]) did not affect tumor growth of PSMA− PC3 flu tumors, as the median survival of the tumor-bearing mice was 9, 14, 11, 11, and 13 d, respectively. On the other hand, median survival compared with untreated controls for animals harboring PSMA+ PC3 PIP tumors at doses of 0 MBq (0 µCi; saline), 0.24 MBq (6.5 µCi), 0.74 MBq (20 µCi), 1.48 MBq (40 µCi), or 3.7 MBq (100 µCi) were 11 (not statistically significant), 27 ($P = 0.0015$), 39 ($P = 0.0005$), 29 ($P = 0.0005$), and not reached ($P = 0.0005$), respectively, indicating that ^{211}At-3-Lu was capable of PSMA-specific tumor growth control and enhancement of survival (Fig. 6). We also tested the efficacy of a single dose of intravenously administered ^{211}At-3-Lu for treating metastatic deposits of PSMA-expressing tumors. Higher doses (1.48 and 3.7 MBq) provided survival benefits compared with the untreated group (Fig. 6B). Median survival for animals treated with 0 MBq (0 µCi; saline), 0.186 MBq (5 µCi), 0.373 MBq (10 µCi), 0.74 MBq (20 µCi), 1.48 MBq (40 µCi), or 3.7 MBq (100 µCi) were 48, 49 (not statistically significant), 48 ($P = 0.5769$, not statistically significant), 52 ($P = 0.0699$, not statistically significant), 57, ($P = 0.0286$), and 58.5 d ($P = 0.2718$, due to an early mouse death), respectively.

Long-Term Radiotoxicity

Eleven-week-old male CD1 mice were injected with 0.24 MBq (6.6 µCi), 0.74 MBq (20 µCi), or 1.48 MBq (40 µCi) of ^{211}At-3-Lu as a single intravenous injection. We also included an untreated group for the entire duration of the study as an age-matched control. All groups of mice consistently gained weight for the 13-mo period of monitoring (Supplemental Fig. 3). Blood chemistry data
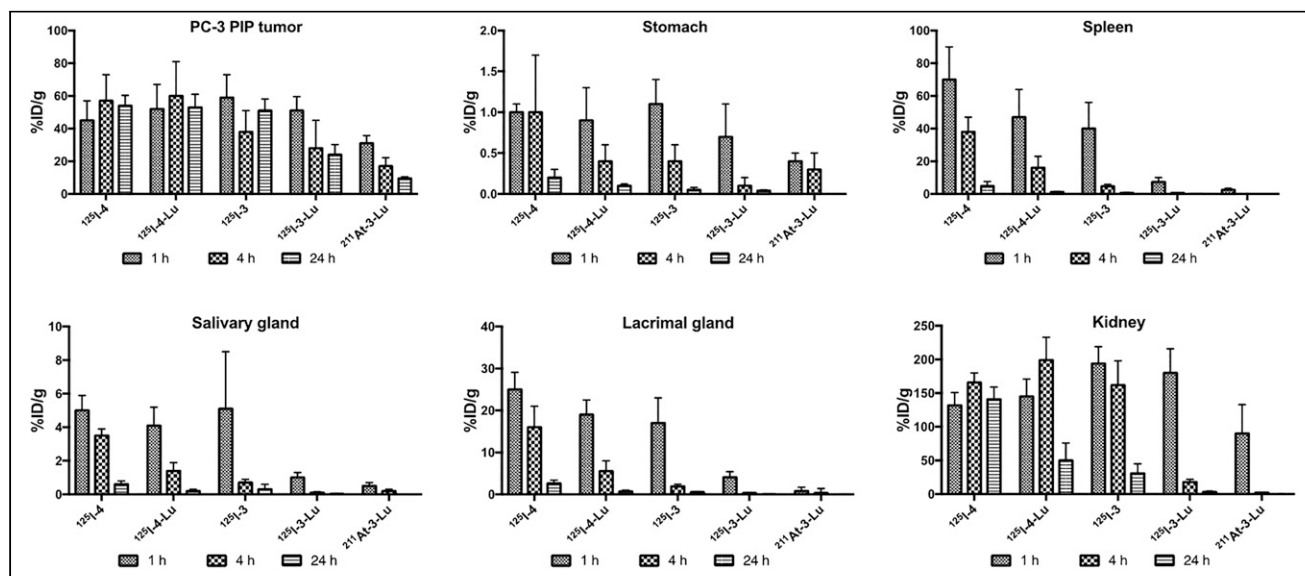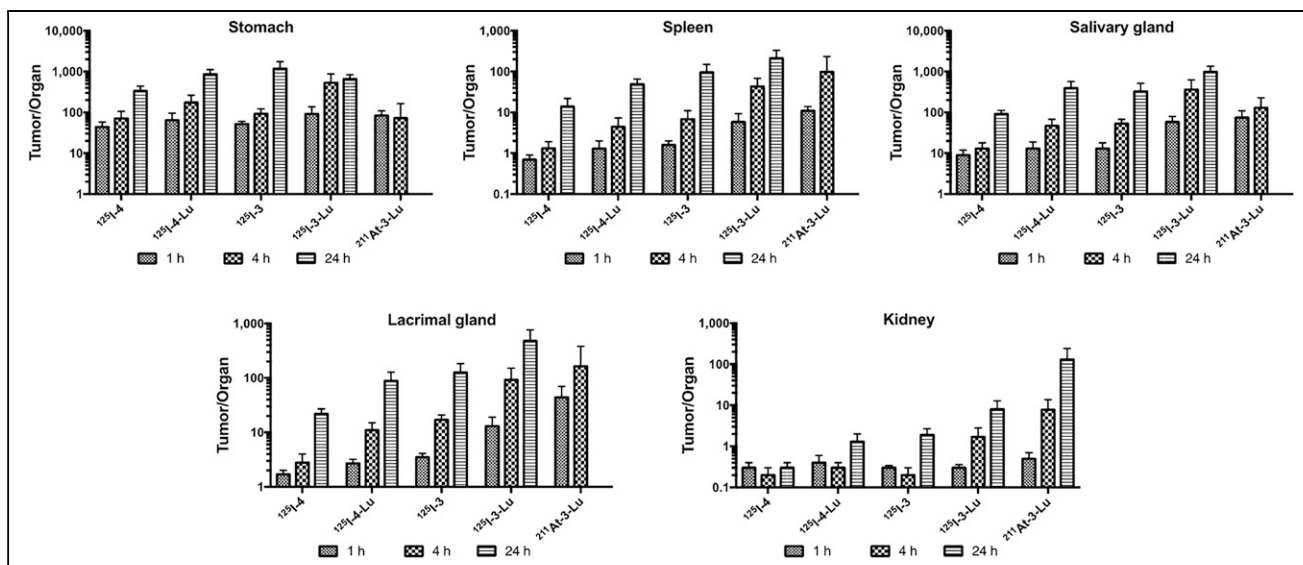

FIGURE 4. Biodistribution (%ID/g) of radiolabeled compounds of Figures 2 and 3 in selected tissues.

FIGURE 5. Biodistribution (ratios of tumor to selected organs) of compounds of Figures 2 and 3 in selected tissues.

for creatinine, blood urea nitrogen, glucose, alkaline phosphatase, alanine aminotransferase, and total protein for all treated groups were similar to those for age-matched untreated controls (Supplemental Fig. 4). A complete blood count also indicated that treated groups remained within normal limits (Supplemental Fig. 4). Monthly evaluation of urine protein level (Supplemental Table 7) and specific gravity (Supplemental Table 8) showed no sign of renal impairment compared with untreated controls for the duration of the study. Histopathologic examination of kidneys, salivary glands, and lacrimal glands revealed no treatment-specific pathologic abnormalities at any dose studied (Fig. 7). We observed mild inflammation, a few dilated tubules with protein deposits, and mild multifocal fibrosis in kidneys from all groups (including controls), which were age-related phenomena. Mild age-related inflammation was also observed in salivary and lacrimal glands from all groups.

DISCUSSION

Banerjee et al. reported a series of 4-halobenzyl derivatives of Lys-Glu-urea inhibitors of PSMA containing a linking group that connects the PSMA-targeting urea pharmacophore with a metal chelator (29). Two of the most promising compounds were 1 and 2 (Fig. 1). When ^{177}Lu-1 and ^{177}Lu-2 were administered intravenously to tumor-bearing mice, they exhibited high uptake in PSMA+ PC3 PIP tumor xenografts (29), low uptake in the

FIGURE 6. Kaplan–Meier curves showing survival in flank (A) and PC3-ML-Luc experimental metastatic (B) models at dose provided. PC3-PIP = PSMA+ PC3 PIP tumors; PC3-flu = PSMA– PC3 flu cell–derived tumors.

salivary glands, rapid renal clearance, and dose-dependent tumor growth delay. We previously demonstrated in a head-to-head preclinical study that our scaffold bearing the β-particle emitter ^{177}Lu was inferior to that delivering ^{225}Ac, an α-emitter, providing a rationale for our focus on PSMA-targeted compounds bearing an α-emitting warhead (30).

Reports of PSMA-targeted therapy with the α-emitter ^{225}Ac-PSMA-617 have been encouraging, even in late-stage disease. Some trials reported PSA declines of at least 90% in roughly half of patients (31) and overall survival of more than 15 mo (32). Such results may exceed those of new chemo- or hormonal therapies. However, those results have come at the costs of decreased quality of life, including nontransient, treatment-halting xerostomia and substantial hematologic toxicity, according to 1 retrospective trial (33). A greater mitigation of off-target effects, which has proved challenging to date, is needed for PSMA-targeted radiopharmaceutical therapy to develop a niche in the management of prostate cancer. Two ways to do so are by optimizing the pharmacokinetics and choosing the correct α-particle emitter. We have attempted both by focusing on the type II Lys-Glu-urea scaffold we have previously reported (29), a close structural analog of which is currently under investigation in a phase 1–2 clinical trial (NCT0349083800), and on using ^{211}At, which produces only 1 α-particle per decay and has a tractable physical half-life of 7.2 h (34–37).

For convenience of handling, we initially studied the ^{125}I-labeled surrogates of the intended ^{211}At compounds to gauge pharmacokinetics and in vivo stability. Compounds of the 4 series (Fig. 3) enabled us to explore the effect of halogen location in the molecule on pharmacokinetics, as well as the influence of a metal within the chelator, which we previously showed enhanced affinity for PSMA (29). Although ^{125}I-**4** and ^{125}I-**4**-Lu behaved similarly in PSMA+ PC3 PIP tumor, ^{125}I-**4**-Lu in kidney substantially decreased by 24 h, indicating a
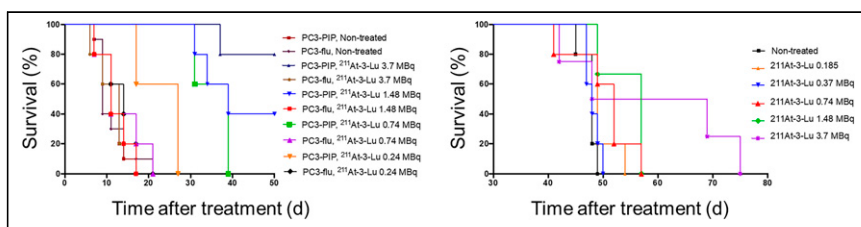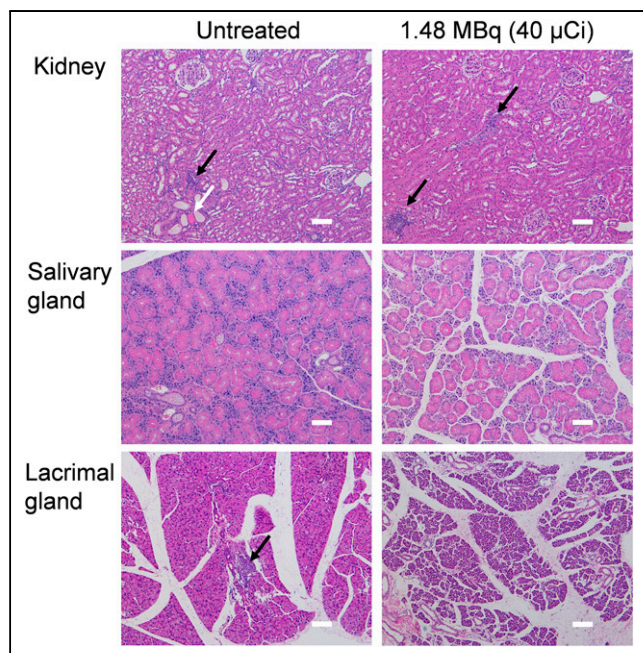
FIGURE 7. Representative microscopic images of kidney, salivary gland, and lacrimal gland (size bar, 100 μm). Black arrows indicate inflammation; white arrow indicates dilated tubule with protein deposit.

positive effect of the presence of lutetium in the chelator on renal clearance. Because even higher tumor-to-kidney ratios were observed for [125]I-**3**-Lu than for [125]I-**4**-Lu, we continued with the former for further in vivo testing. Relative to [125]I-**3**-Lu, [211]At-**3**-Lu demonstrated lower tumor uptake but also lower off-target uptake. There was also moderate uptake within stomach, consistent with some deastatination (38); however, levels remained below 0.5 %ID/g and tumor-to-stomach ratios were approximately 100 (Figs. 4 and 5). By contrast, [211]At-DCABzL never had tumor-to-stomach ratios that rose above a few percentage points out to 18 h (18), and a recently published [211]At-labeled minibody targeting prostate cancer had a ratio that only exceeded 1 on treatment with perchlorate at 5 h (1.2) and 9 h (1.4) after injection (39).

The lack of uptake within stomach and salivary glands of [211]At-**3**-Lu could in part be due to the stability of the low-molecular-weight, Lys-Glu-urea–based targeting scaffold (40). There was also little radioactivity in blood (Supplemental Table 3) and no significant change in white blood cell counts (Supplemental Fig. 4). Accordingly, neither treatment with perchlorate (39) nor blocking agents were required to mitigate off-target effects. In vivo, [211]At-**3**-Lu treatment caused a PSMA- and dose-dependent increase in survival compared with control animals in both the flank and metastatic models (Fig. 6). Comparison of this result with other reported compounds is challenging because of the different model systems used. If we focus on our own earlier therapy studies, we find that [211]At-**3**-Lu provided survival effects at much lower doses than [211]At-DCABzL (18), which had a maximum tolerated dose (MTD) of 37 kBq (1 μCi). However, that study was performed on nude rather than SCID mice, which we used here. We did not reach the MTD for [211]At-**3**-Lu, as the highest dose administered in the long-term (13 mo) toxicity study with normal mice was only 1.48 MBq (40 μCi). Nonetheless, even at a dose up to 40 times higher than the MTD for [211]At-DCABzL in the same mouse strain, our toxicity data showed only mild changes at all

doses and in all organs studied (Fig. 7). Perhaps a more relevant comparison is to [225]Ac-L1 (30), which demonstrated an MTD of 9.3 kBq (0.25 μCi) (fractionated × 4) because the scaffold is the same as that of [211]At-**3**-Lu. Compound [212]Pb-L2 (41), which has a similar scaffold, demonstrated an MTD of 1.5 MBq (~40 μCi). For that compound, there were concerns of long-term renal toxicity, which may be due to the [212]Bi daughter released and localized to the kidney, which is not a problem with [211]At-based agents.

Our goal in this work was to find a suitable α-particle–emitting agent to treat PSMA+ prostate and other cancers that had minimal off-target toxicity, namely, an agent that would be more effective than the corresponding β-particle emitter but not as toxic as those radiolabeled with [225]Ac. We have achieved that with [211]At-**3**-Lu, attesting to the potential benefits of this potentially tamer α-emitter. As with [212]Pb, [211]At emits only 1 α-particle per decay. As such, these 2 radionuclides do not produce daughter α-emissions outside the intended target site and will not be expected to have the toxicity—for example, in liver—attendant on such emissions, such as those seen with [225]Ac. However, there are differences between [212]Pb and [211]At that make us favor the latter. The therapeutic potential of [212]Pb will be diminished if the daughter nuclei do not remain at the target site so that their energy can also be captured (7). For example, Ackerman et al. have calculated that migration of daughters with [212]Pb could reduce its relative biological effectiveness to that of conventional external-beam radiation and β-particle emitters (42). Furthermore, [211]At can be introduced to targeting ligands using chemistry very similar to that for other halogens to minimize perturbation of the targeting scaffold if a fastidious cellular target is sought, or a chelator can be deliberately introduced to enhance pharmacokinetics, as in this case (36,37). Lack of off-target toxicity, including to salivary and lacrimal glands, would obviate cumbersome coadministration of blocking agents. However, although the natural bismuth target material is inexpensive and widely available, [211]At requires a 28-MeV α-particle cyclotron beam for efficient production—a requirement that has curtailed its use (43). There are concerted efforts under way to increase the supply of [211]At worldwide at academic institutions and research institutes, with commercial sources emerging in the not-too-distant future (https://ionetix.com/why-alpha-therapy).

A limitation of this study was the use of cells that may not reflect the natural abundance and heterogeneity of PSMA in human cancer. That issue has been discussed in detail elsewhere (44). However, PSMA+ PC3 PIP and PSMA− PC3 flu cells have the advantage of being isogenic, except for PSMA expression, enabling us to answer questions about pharmacokinetics with a minimum of variables present. The superior performance of [211]At-**3**-Lu in the flank model rather than the metastatic model may reflect, in part, the supraphysiologic and 10-fold higher PSMA expression in the PSMA+ PC3 PIP cells relative to the PSMA+ PC3-ML-Luc cells used to generate the metastatic deposits (18), which express PSMA at about the same level of LNCaP cells (27).

CONCLUSION

In this small series, [211]At-**3**-Lu proved to have an excellent combination of properties: a pharmacokinetic profile matching the physical half-life of [211]At, the ability to improve survival in tumor-bearing animals, and lack of off-target toxicity as demonstrated by hematopoietic stability, unchanged tissue chemistries, weight gain rather than loss throughout treatment, and favorable

histopathology. This compound or close analogs are promising for translation if and when an α-particle emitter is to be considered in the therapeutic journey of the patient.

KEY POINTS

QUESTION: Can a PSMA-targeted, α-emitting small molecule be designed with few off-target toxic effects while retaining therapeutic efficacy?

PERTINENT FINDINGS: Lead compound [211]At-**3**-Lu was able to control tumor growth and enhance survival in animals treated at doses of 1.48 MBq or greater and did so without toxicity.

IMPLICATIONS FOR PATIENT CARE: Compounds such as [211]At-**3**-Lu provide a further rationale for the use of [211]At in targeted α-emitting radiopharmaceuticals. [211]At may be an effective and nontoxic alternative to other α-emitters in use for management of prostate and other PSMA-expressing cancers. Its ease of incorporation in a variety of cancer affinity agents, including small molecules, as well as its convenient physical half-life could provide a safe, practical, and new method to treat a variety of intractable malignancies.

REFERENCES

1. Miyahira AK, Pienta KJ, Babich JW, et al. Meeting report from the Prostate Cancer Foundation PSMA Theranostics State of the Science meeting. *Prostate.* 2020; 80:1273–1296.
2. Jones W, Griffiths K, Barata PC, Paller CJ. PSMA theranostics: review of the current status of PSMA-targeted imaging and radioligand therapy. *Cancers (Basel).* 2020;12:1367.
3. O'Dwyer E, Bodei L, Morris MJ. The role of theranostics in prostate cancer. *Semin Radiat Oncol.* 2021;31:71–82.
4. Zechmann CM, Afshar-Oromieh A, Armor T, et al. Radiation dosimetry and first therapy results with a [124]I/^{131}I-labeled small molecule (MIP-1095) targeting PSMA for prostate cancer therapy. *Eur J Nucl Med Mol Imaging.* 2014;41:1280–1292.
5. Kratochwil C, Giesel FL, Stefanova M, et al. PSMA-targeted radionuclide therapy of metastatic castration-resistant prostate cancer with ^{177}Lu-labeled PSMA-617. *J Nucl Med.* 2016;57:1170–1176.
6. Morgenstern A, Apostolidis C, Kratochwil C, Sathekge M, Krolicki L, Bruchertseifer F. An overview of targeted alpha therapy with [225]actinium and [213]bismuth. *Curr Radiopharm.* 2018;11:200–208.
7. Dos Santos JC, Schafer M, Bauder-Wust U, et al. Development and dosimetry of [203]Pb/[212]Pb-labelled PSMA ligands: bringing "the lead" into PSMA-targeted alpha therapy? *Eur J Nucl Med Mol Imaging.* 2019;46:1081–1091.
8. Hammer S, Hagemann UB, Zitzmann-Kolbe S, et al. Preclinical efficacy of a PSMA-targeted thorium-227 conjugate (PSMA-TTC), a targeted alpha therapy for prostate cancer. *Clin Cancer Res.* 2020;26:1985–1996.
9. Kratochwil C, Bruchertseifer F, Giesel FL, et al. [225]Ac-PSMA-617 for PSMA-targeted alpha-radiation therapy of metastatic castration-resistant prostate cancer. *J Nucl Med.* 2016;57:1941–1944.
10. Yadav MP, Ballal S, Sahoo RK, Tripathi M, Seth A, Bal C. Efficacy and safety of [225]Ac-PSMA-617 targeted alpha therapy in metastatic castration-resistant prostate cancer patients. *Theranostics.* 2020;10:9364–9377.
11. Hofman MS, Violet J, Hicks RJ, et al. [^{177}Lu]-PSMA-617 radionuclide treatment in patients with metastatic castration-resistant prostate cancer (LuPSMA trial): a single-centre, single-arm, phase 2 study. *Lancet Oncol.* 2018;19:825–833.
12. Zacherl MJ, Gildehaus FJ, Mittlmeier L, et al. First clinical results for PSMA-targeted α-therapy using 225Ac-PSMA-I&T in advanced-mCRPC patients. *J Nucl Med.* 2021;62:669–674.
13. Ilhan H, Gosewisch A, Boning G, et al. Response to [225]Ac-PSMA-I&T after failure of long-term ^{177}Lu-PSMA RLT in mCRPC. *Eur J Nucl Med Mol Imaging.* 2021; 48:1262–1263.
14. de Kruijff RM, Wolterbeek HT, Denkova AG. A critical review of alpha radionuclide therapy: how to deal with recoiling daughters? *Pharmaceuticals (Basel).* 2015;8:321–336.
15. Kozempel J, Mokhodoeva O, Vlk M. Progress in targeted alpha-particle therapy: what we learned about recoils release from in vivo generators. *Molecules.* 2018; 23:581.
16. Palm S, Humm JL, Rundqvist R, Jacobsson L. Microdosimetry of astatine-211 single-cell irradiation: role of daughter polonium-211 diffusion. *Med Phys.* 2004;31: 218–225.
17. Bismuth-207. U.S. Nuclear Regulatory Commission website. https://www.nrc.gov/reading-rm/doc-collections/cfr/part020/appb/bismuth-207.html. Updated March 24, 2021. Accessed August 11, 2021.
18. Kiess AP, Minn I, Vaidyanathan G, et al. (2S)-2-(3-(1-carboxy-5-(4-[211]At-astato-benzamido)pentyl)ureido)-pentanedioic acid for PSMA-targeted alpha-particle radiopharmaceutical therapy. *J Nucl Med.* 2016;57:1569–1575.
19. Vaidyanathan G, Mease RC, Minn I, et al. Synthesis and preliminary evaluation of [211]At-labeled inhibitors of prostate-specific membrane antigen for targeted alpha particle therapy of prostate cancer. *Nucl Med Biol.* 2021;94–95:67–80.
20. Sessler JL, Wang B, Harriman A. Photoinduced energy transfer in associated but noncovalently linked Photosynthetic model system. *J Am Chem Soc.* 1995;117: 704–714.
21. Maresca KP, Hillier SM, Femia FJ, et al. A series of halogenated heterodimeric inhibitors of prostate specific membrane antigen (PSMA) as radiolabeled probes for targeting prostate cancer. *J Med Chem.* 2009;52:347–357.
22. Vaidyanathan G, White BJ, Affleck DJ, et al. SIB-DOTA: a trifunctional prosthetic group potentially amenable for multi-modal labeling that enhances tumor uptake of internalizing monoclonal antibodies. *Bioorg Med Chem.* 2012;20:6929–6939.
23. Zalutsky MR, Zhao XG, Alston KL, Bigner D. High-level production of alpha-particle-emitting [211]At and preparation of [211]At-labeled antibodies for clinical use. *J Nucl Med.* 2001;42:1508–1515.
24. Pozzi OR, Zalutsky MR. Radiopharmaceutical chemistry of targeted radiotherapeutics, part 3: alpha-particle-induced radiolytic effects on the chemical behavior of [211]At. *J Nucl Med.* 2007;48:1190–1196.
25. Chang SS, Reuter VE, Heston WD, Bander NH, Grauer LS, Gaudin PB. Five different anti-prostate-specific membrane antigen (PSMA) antibodies confirm PSMA expression in tumor-associated neovasculature. *Cancer Res.* 1999;59:3192–3198.
26. Nakajima T, Mitsunaga M, Bander NH, Heston WD, Choyke PL, Kobayashi H. Targeted, activatable, in vivo fluorescence imaging of prostate-specific membrane antigen (PSMA) positive tumors using the quenched humanized J591 antibody-indocyanine green (ICG) conjugate. *Bioconjug Chem.* 2011;22: 1700–1705.
27. Kiess AP, Minn I, Chen Y, et al. Auger radiopharmaceutical therapy targeting prostate-specific membrane antigen. *J Nucl Med.* 2015;56:1401–1407.
28. Jackson PF, Cole DC, Slusher BS, et al. Design, synthesis, and biological activity of a potent inhibitor of the neuropeptidase N-acetylated alpha-linked acidic dipeptidase. *J Med Chem.* 1996;39:619–622.
29. Banerjee SR, Kumar V, Lisok A, et al. ^{177}Lu-labeled low-molecular-weight agents for PSMA-targeted radiopharmaceutical therapy. *Eur J Nucl Med Mol Imaging.* 2019;46:2545–2557.
30. Banerjee SR, Lisok A, Minn I, et al. Preclinical evaluation of [213]Bi- and [225]Ac-labeled low-molecular-weight compounds for radiopharmaceutical therapy of prostate cancer. *J Nucl Med.* 2021;62:980–988.
31. Sathekge M, Bruchertseifer F, Knoesen O, et al. [225]Ac-PSMA-617 in chemotherapy-naive patients with advanced prostate cancer: a pilot study. *Eur J Nucl Med Mol Imaging.* 2019;46:129–138.

32. Sathekge M, Bruchertseifer F, Vorster M, et al. Predictors of overall and disease-free survival in metastatic castration-resistant prostate cancer patients receiving [225]Ac-PSMA-617 radioligand therapy. *J Nucl Med.* 2020;61:62–69.

33. Feuerecker B, Tauber R, Knorr K, et al. Activity and adverse events of actinium-225-PSMA-617 in advanced metastatic castration-resistant prostate cancer after failure of lutetium-177-PSMA. *Eur Urol.* 2021;79:343–350.

34. Lindegren S, Albertsson P, Back T, Jensen H, Palm S, Aneheim E. Realizing clinical trials with astatine-211: the chemistry infrastructure. *Cancer Biother Radiopharm.* 2020;35:425–436.

35. Meyer GJ. Astatine. *J Labelled Comp Radiopharm.* 2018;61:154–164.

36. Vaidyanathan G, Zalutsky MR. Astatine radiopharmaceuticals: prospects and problems. *Curr Radiopharm.* 2008;1:177.

37. Guérard F, Gestin JF, Brechbiel MW. Production of [211At]-astatinated radiopharmaceuticals and applications in targeted alpha-particle therapy. *Cancer Biother Radiopharm.* 2013;28:1–20.

38. Larsen RH, Slade S, Zalutsky MR. Blocking [211At]astatide accumulation in normal tissues: preliminary evaluation of seven potential compounds. *Nucl Med Biol.* 1998;25:351–357.

39. Bäck TA, Jennbacken K, Hagberg Thulin M, et al. Targeted alpha therapy with astatine-211-labeled anti-PSCA A11 minibody shows antitumor efficacy in prostate cancer xenografts and bone microtumors. *EJNMMI Res.* 2020;10:10.

40. Pomper MG, Musachio JL, Zhang J, et al. ^{11}C-MCG: synthesis, uptake selectivity, and primate PET of a probe for glutamate carboxypeptidase II (NAALADase). *Mol Imaging.* 2002;1:96–101.

41. Banerjee SR, Minn I, Kumar V, et al. Preclinical evaluation of [203]/[212]Pb-labeled low-molecular-weight compounds for targeted radiopharmaceutical therapy of prostate cancer. *J Nucl Med.* 2020;61:80–88.

42. Ackerman NL, de la Fuente Rosales L, Falzone N, Vallis KA, Bernal MA. Targeted alpha therapy with [212]Pb or [225]Ac: change in RBE from daughter migration. *Phys Med.* 2018;51:91–98.

43. Zalutsky MR, Pruszynski M. Astatine-211: production and availability. *Curr Radiopharm.* 2011;4:177–185.

44. Current K, Meyer C, Magyar CE, et al. Investigating PSMA-targeted radioligand therapy efficacy as a function of cellular PSMA levels and intratumoral PSMA heterogeneity. *Clin Cancer Res.* 2020;26:2946–2955.